Geophysical Inversion of Thermospheric Winds at 250km Altitude using higher order Tikhonov Regularization on the Alaskan Allsky Fabry-Perot Interferometry Network for the night of Jan 31st,2016.

John Elliott and Mark Conde
Geophysical Institute, University of Alaska Fairbanks

Motivation

The Alaskan Network is comprised of four Allsky implemented Fabry-Perot Interferometers, called Scanning Doppler Imagers (SDIs). Each SDI measures 115 temporally simultaneous spatially independent spectra of atomic oxygen via atmospheric nightglow and auroral emission centered about 6300Å, with a spectral resolution of ± 0.01pm[1, 2, 3]. The SDI converts these raw measurements into processed line of sight (LOS) observations with a corresponding resolution of $\pm 5\frac{m}{s}$. When all Alaskan instruments are observed together they have spatial overlap.

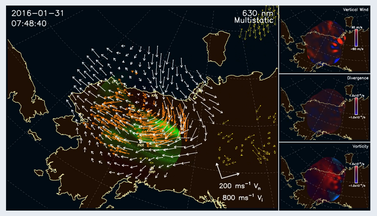

Figure 1: Thermospheric wind reconstruction over Alaska on Jan 31st, 2016 during high auroral activity. Orange arrows are direct trigonometric reconstruction while white arrows are basis function fitting method. Yellow arrows are superDARN measured ion velocities dragging nuetral winds and introducing small scale structure.

On the night of January 31st, 2016 there were three SDIs recording data, totaling 345 near temporally simultaneous measurements over approximately one square megameter of Alaska with a cadence of about 5min per measurement set. Two other wind inference methods have been applied on data for this night (figure 1), and ion convection (superDARN) data is available as well.

It is our goal to provide a new method of inferring wind by means of geophysical inversion that captures large scale features in agreement with existing methods and also additionally globally resolves small scale features that are yet to be studied in detail in the thermosphere.

The Forward Model

The Alaskan SDIs record temporally nearly-simultaneous and geographically overlapping LOS data. Geometrically a LOS observation, d_i, is the projection of the subtended wind vector field $\vec{u_i}$ components onto the look direction $\vec{r_i}$ in which the observation is made.

$$d_i = \frac{\vec{u_i} \cdot \vec{r_i}}{r_i} = \sum_{j=1}^{3} \frac{u_{i_j} x_j}{r_i} \tag{1}$$

$$d_i = u_{i_x} \sin\theta_i \sin\phi_i + u_{i_y} \sin\theta_i \cos\phi_i + u_{i_z} \cos\theta_i \tag{2}$$

With θ_i being the angle from zentih and ϕ_i is the azimuthal angle clockwise from North for a given observation. A linearized design matrix G is constructed that performs the geometrical transformation for each observation described by equation 1. G is made sparse such that an entire wind field $\vec{u}$ can act on a observation basis in G and perform the equivalent operation described in equation 1[4]. G will thus have dimensions $\{M,3N^2\}$ for a system with M observations reconstructed on a grid of size $\{N,N,3\}$. To accomplish this we vectorize the three dimensional wind field such that:

$$G_i = \langle \dots \sin\theta_i \sin\phi_i \dots \sin\theta_i \cos\phi_i \dots \cos\theta_i \dots \rangle$$
$$\vec{u} = \left\langle u_{1_x}, ..., u_{N_x}, u_{1_y}, ..., u_{N_y}, ..., u_{1_z}, ..., u_{N_z} \right\rangle^T \tag{3}$$

Where G_i contains the geometrical components necessary to satisfy equation 1 at the location corresponding to the grid element or is zero elsewhere. We now have the forward model:

$$d_\alpha = G_\alpha^\beta u_\beta \tag{4}$$

The contraction described in equation 4 is the equation of an observation by the inner product of the two observation vectors in equations 3.

Solid Angle Correction

Equation 4 assumes d_i is observed (mathematically) from a single vector in a vector field, over an infinitesimal solid angle. Our SDI measures the average wind field over a defined solid angle $d\Omega$. A correction to equation 4 is needed.

To correct this, in practice, an equiareal Gaussian solid angle projection is assumed. The design matrix is then corrected by spatially convolving an appropriately sized Gaussian kernel κ with each direction (zonal,meridional,vertical) of a design matrix row G_i reshaped to {N,N}:

$$G_{corrected} = \kappa(x,y) \star G(x,y) =$$
$$\iint_{\Re^2} \kappa(\tau_1, \tau_2) \cdot G(x-\tau_1, y-\tau_2) d\tau_1 d\tau_2 \tag{5}$$

The convolution in equation 5 drops the condition number of G stabilizing the inverse problem[5]. A fully independent treatment of solid angle per element can be applied using conic sections and the phenomena altitude of 250km. This paper uses equation 5 for all computations.

Inverse Theory

The projection of a vector field to a LOS measurement is a surjective mapping $\mathbb{R}^3 \to \mathbb{R}$ and thus an inverse map is injective and not unique. An infinite number of possible solutions exist given the injective mapping and density of the reals.

Geophysical constraints and/or regularizations must be applied in order to successfully map this inverse problem.

For thermospheric winds a regularized solution is sought by utilization of a generalized Tikhonov set of equations:[a]

$$\vec{u^*} = (\Lambda)^{-1} G^T C_d^{-1} \vec{d} \tag{6}$$
$$\Lambda_\eta^\zeta = G_\eta^\beta C_d^{-1\prime}{}_\beta G_\iota^\zeta + \Psi_\eta^\xi \Psi_\xi^\zeta \tag{7}$$
$$\vec{u} = \min_{\vec{u^*}} \left[||G\vec{u^*} - \vec{d}||^2 + ||\Psi\vec{u^*}||^2 \right] \tag{8}$$

In equation 7 C_d^{-1} is the inverse of the data covariance and Ψ is the regularization term. Ψ Usually takes the form of $\Psi_\epsilon^\gamma = \alpha\delta_\epsilon^\gamma$ adding a zeroth order offset to the inversion in order to stabilize the proceeding inversion. The effect of this is to smooth the eigenspace of the design matrix enough to converge[5].

[a] A working knowledge of Tikhonov Regularization is assumed. See [5, 6] for derivation

Higher Order Regularization

When considering small scale reconstruction of thermospheric wind fields a zeroth order Tikhonov reconstruction alone over-smooths the eigenspace, removing small scale variance[5]. A higher order Ψ is investigated to add correction the zeroth order term:

$$\Psi_\epsilon^\gamma = \beta G_\epsilon^\delta \delta_\delta^\gamma + \alpha\delta_\delta^\gamma \tag{9}$$
$$\Lambda_\eta^\zeta = G_\eta^\beta C_d^{-1\prime}{}_\beta G_\iota^\zeta + \left(\beta G_\eta^\delta + \alpha\right)\delta_\delta^\xi \left(\beta G_\xi^\delta + \alpha\right)\delta_\delta^\zeta \tag{10}$$

The hyper-parameters α, β act on Ψ to allow the zeroth and higher order terms to be tuned independently. The addition of the higher order term is the contraction $G_\epsilon^\delta \delta_\delta^\gamma$ which are interpreted as the strength of observations made from wind field elements γ. This gives preference in reconstruction based on how many data measurements constrain a given wind field, allowing zeroth order smoothing to prevail where there are not many measurements and the measurement reconstruction to prevail otherwise.

Synthetic Data Results

Synthetic data was produced that included a hyperbolic tangentially variable wind field with a normally distributed added noise where one sigma of deviation was less than or equal to 25% of the maximum wind speed. A shear was added meridionally in the center of the wind field (Figure 2).

To validate the performance of the algorithm an inner product metric was used:

$$M = \cos\theta = \frac{\vec{u^*} \cdot \vec{u}_{synth}}{|\vec{u^*}||\vec{u}_{synth}|} \tag{11}$$

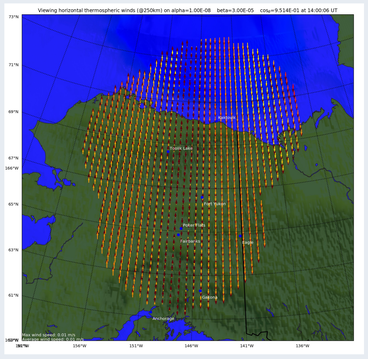

Figure 2: Red arrows are the generated synthetic winds and orange arrows are the reconstructed winds. A metric agreement of over 95% is achieved.

M has a domain $M \in [-1, 1]$, where the most optimal reconstruction is the maximal value of M achieved.

After brute searching the metric (equation 11) maximized at 95% agreement for an optimal α, β. Visually (Figure 2) very strong agreement was observed in the data, with an over-smoothed region about the generated shear line. Sheared sinusoidal, constant, and Gaussian varying wind fields tested at approximately 95% agreement as well.

Real Data Results

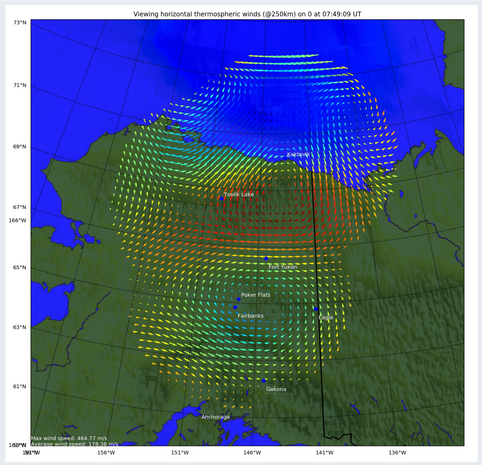

Figure 3: Model reconstruction for same time and location as figure 1. Color of vectors represents vertical wind speed.

Real data was taken from the Alaskan SDI network for the night of January 31st, 2016, utilizing data from Poker Flat, Toolik Field Station, and Kaktovik stations. This resulted in 345 independent LOS measurements with a varying temporal cadence of about 2 minutes. Data covariance was measured and reported by each SDI, along with azimuthal and zenith angles, for each d_i observed. Without in situ verification via rocket missions, the validity of the wind reconstruction relies on other techniques that have previous in situ validation.

For this, we look look at the work of Conde et al (Figure 1) using polynomial basis fitting and direct trigonometric calculation. Large scale structure are observed in general agreement (figure 3). Reconstructions were determined to be physically meaningful. Small scale features are present that agree with direct trigonometric calculations of data (orange arrows, figure 1). Additional observations of small scale phenomena are present, but need more quantitative analysis before determining validity.

Discussion

The reconstruction of synthetic winds produced objectively and subjectively good results. For synthetic data the evaluation metric measured over 95% agreement in reconstruction, providing strong evidence that the methodology is valid for this type of application.

In practice real reconstructions are difficult to measure objectively. Without strong regularization, a reconstructed wind field element where no data was collected can reconstruct in any manner equally as valid as any other. The overall reconstruction attempts to optimize any differences between elements and may indeed find a non-physical artifact valid in order to optimally regularize the known data.

For a heavily regularized region, a typical artifact is a vorticular region absent of any present physical driving mechanism. This artifacting is due to regularization imposed limitations of the model during reconstruction. High curvature elements are not permitted but, being unconstrained by the data and emphasizing smoothness, the zeroth order regularization term often will seek to minimize the divergence of the anomaly and thus produce curling vector fields locally.

Strong physical regularization is needed to constrain the inverse algorithm appropriately. Methods including optimizing variations on the Burnside Condition[7], continuity, and physically reasonable domain constraints have been attempted with acute success.

References

[1] M. Conde and R. W. Smith, "Mapping thermospheric winds in the auroral zone," *Geophys. Res. Lett.*, 1995.

[2] M. Conde and R. W. Smith, "Phase compensation of a separation scanned, all-sky imaging fabry-perot spectrometer for auroral studies," *Appl. Opt.*, 1997.

[3] M. Conde and R. W. Smith, "Spatial structure in the thermospheric horizontal wind above poker flat, alaska, during solar minimum," *J. Geophys. Res.*, 1998.

[4] B. J. Harding, J. J. Makela, and J. W. Meriwether, "Estimation of mesoscale thermospheric wind structure using a network of interferometers," *J. Geophys. Res. Space Physics*, 2015.

[5] R. Aster, *Parameter Estimation and Inverse Problems.* Academic Press, 2nd ed., 2012.

[6] A. Tarantola, *Inverse Problem Theory.* SIAM, 1st ed., 2005.

[7] S. L. Cooper, M. Conde, and P. Dyson, "Numerical simulations of thermospheric dynamics: divergence as a proxy for vertical winds," *Ann. Geophys.*, 2009.